NICST_MEMO_11_008

NICST Internal Memo

Date: July 6, 2011
From: Jeff McIntire
To: Bruce Guenther, Jim Butler, and Jack Xiong
Subject: Solar Diffuser Measurements from End-to-End Testing of the Reflective Solar Bands Using T-SIRCUS

References:

[1] 'Facility for Spectral Irradiance and Radiance Responsivity Calibrations Using Uniform Sources,' S. W. Brown, G. P. Eppeldauer, and K. R. Lykke, Appl. Opt 45(32), 8218-8237 (2006).
[2] NICST_MEMO_08_007, 'Drift Corrected VIIRS FU1 Response Versus Scan (RVS) for the Reflective Solar bands (RSB) from FP-10 Test,' C. Pan and N. Che, March 3, 2008.
[3] NICST_MEMO_08_043, 'VIIRS FU1 SD Prelaunch BRF for Both VIIRS and SDSM Views,' J. Sun and S. Xiong, December 17, 2008.
[4] 'NIST Laser Collimator Non-Uniformity Corrections for VIIRS End-to-End Test,' J. McCarthy, April 6, 2010.
[5] *An Introduction to Error Analysis*, J. R. Taylor, University Science Books (1997).
[6] 'Performance Verification Report – VIIRS FU1 Reflective band Calibration (PVP Section 4.2.2),' B. Robinson, M. Bliton, R. Menzel, and D. Tyler, December 3, 2009.

1. Introduction

The End-to-End (E2E) test of the RSB calibration cycle was performed in March 2010 at the BATC facility in Boulder CO. The VIIRS F1 sensor had been integrated into the NPP spacecraft in January 2010. E2E testing utilized the NIST T-SIRCUS as a source [1].

This memo will describe the analysis of the E2E measurement of the SD calibration cycle (the SDSM measurements will be discussed in a separate memo). Table 1 lists the data used in this work.

2. Analysis Methodology

2.1 Test Description

T-SIRCUS consists of a series of tunable lasers; for E2E testing, a Ti:sapphire laser was used in continuous wave mode to produce monochromatic illumination at 742 and 852 nm (and frequency doubling was used to reach 442 nm) [1].

The T-SIRCUS was used to feed two sources via fiber optics: an integrating sphere and a collimator. The integrating sphere was positioned in the EV at a scan angle of ~ -0.2 degrees (VIIRS nadir view is defined as 0 degrees). Two radiance monitors were used to track the radiance output from the sphere in real-time. The monitors were positioned just off the optical path, one above and one below. NIST provided calibration coefficients (determined post-test) were used to convert the monitor output from volts to radiance.

The collimator was positioned to illuminate both the SD view and the SDSM solar view. The exit aperture of the collimator was about 25 inches in diameter. A total of seven collimator positions were performed covering five different angles, listed in Table 1 in the order performed. Note that the first, fourth, and fifth positions were repeated measurements of roughly the same angle. An irradiance monitor was positioned near the center of the collimator exit aperture, from which real-time tracking of the irradiance was performed. NIST provided calibration coefficients were used to convert the monitor output from volts to irradiance.

VIIRS data for E2E testing was recorded in a three data collect cycle. During the first collect, the SD and SDSM were illuminated, while the EV was dark. For the second collect, the EV was illuminated, while the SD and SDSM views were dark. For the last collect, both the EV and SD views were dark. Each of these collects contained 128 VIIRS scans (roughly 3.8 minutes) in diagnostic mode. For most collimator positions, this cycle was conducted twice per measured wavelength (except position 5 when it was conducted only once). Data collects were recorded with the SIRCUS output at 442, 742, and 852 nm (442 nm was only measured once during collimator position 7); this corresponds to VIIRS bands M2, M6, and M7 (see Table 1).

2.2 Responsivity Determination

Ideally, the responsivities determined using the SD or EV paths should be equal. As a result, the metric of interest for this portion of the E2E test is the responsivity ratio, or

$$\eta = \frac{g_{SD}}{g_{EV}}. \tag{1}$$

Here the g_{SD} and g_{EV} are the responsivities of the SD and EV paths.

The responsivity from the EV path is

$$g_{EV} = \frac{dn_{EV}}{RVS_{EV} L_{EV}}. \tag{2}$$

The RVS was determined in [2] (for this test the EV HAM AOI was ~36.3 degrees). The radiance is the average of the two monitor radiances on the integrating sphere.

The responsivity from the SD path is

$$g_{SD} = \frac{\pi dn_{SD}}{\gamma_1 E_{mon} \tau_{SAS} BRF_{RTA} \cos \vartheta_{SD}}. \tag{3}$$

The $\cos\theta_{SD}$ is the cosine of the projection angle for the incident irradiance on the SD; it is defined as the dot product of the SD normal vector (0.29724, -0.21860, 0.92944) and the sun vector

$$\vec{n}_{sun} = \frac{1}{\sqrt{1+\tan^2\phi+\tan^2\delta}}(1,-\tan\phi,\tan\delta). \tag{4}$$

Here δ and φ are the collimator declination and azimuthal angles, respectively. τ_{SAS} is the transmission of the solar attenuation screen, which is given by

$$\tau_{SAS} = 0.1258(1-0.1538\tan\delta)(1-0.04746\tan\phi). \tag{5}$$

The BRF was fit to a quadratic polynomial in both declination and azimuthal angles [3], or

$$BRF_{RTA} = c_0 + c_1\delta + c_2\phi + c_3\delta^2 + c_4\phi^2 + c_5\delta\phi, \tag{6}$$

where the coefficients were determined at wavelengths 400, 500, 600, 700, and 900 nm. The BRF used here is interpolated between the two nearest wavelengths. E_{mon} is the collimator monitor irradiance and γ_1 is the collimator uniformity correction [4] (listed in Table 2). In addition, the RVS has been normalized to the SD HAM AOI of ~60.2 degrees [2].

2.3 Uncertainty Analysis

The uncertainty in the responsivity ratio is defined by the standard error propagation [5] as

$$\frac{u^2(\eta)}{\eta^2} = \frac{u^2(g_{SD})}{g_{SD}^2} + \frac{u^2(g_{EV})}{g_{EV}^2}. \tag{7}$$

The uncertainty in the EV responsivity is expressed by the following:

$$\frac{u^2(g_{EV})}{g_{EV}^2} = \frac{u^2(dn_{EV})}{dn_{EV}^2} + \frac{u^2(RVS_{EV})}{RVS_{EV}^2} + \frac{u^2(L_{EV})}{L_{EV}^2}. \tag{8}$$

The uncertainty in the dn_{EV} is the standard deviation over all samples and scans for a particular measurement (all known biases that effect the dn have been removed). The RVS uncertainty is taken from [2]. The L_{EV} uncertainty is the RSS of the standard deviation of L_{EV} over scans and the average offset between the two radiance monitor outputs.

The uncertainty in the SD responsivity is defined by the following:

$$\frac{u^2(g_{SD})}{g_{SD}^2} = \frac{u^2(dn_{SD})}{dn_{SD}^2} + \frac{u^2(RVS_{SD})}{RVS_{SD}} + \frac{u^2(\tau_{SAS})}{\tau_{SAS}} + \frac{u^2(BRF_{RTA})}{BRF_{RTA}} + \frac{u^2(E_{mon})}{E_{mon}^2} + \frac{u^2(\gamma_1)}{\gamma_1} + \frac{u^2(\cos\theta_{SD})}{\cos^2\theta_{SD}}. \tag{9}$$

The dn_{SD} and RVS uncertainties are determined in the same manner as above [2]. τ_{SAS} and BRF_{RTA} uncertainties were determined by the sensor vendor [6] (0.24 % and 1.09 %, respectively). The uncertainty in E_{mon} is the standard deviation of E_{mon} over scans. The error in the cosine of the projection angle was determined by propagating an uncertainty of 0.01 degrees for each angle through the dot product of Eq. (4) and the SD normal vector. At present, the uncertainty of the collimator uniformity correction is undetermined. This analysis assumes that there are no covariance terms between the individual uncertainty terms (as the contributors were measured separately).

3. Analysis Results

3.1 Data Reduction

The integrating sphere aperture covered an arc of about 2 degrees of scan angle centered roughly on nadir. From this region, 90 moderate resolution (750 m) samples were extracted (samples 970-1059). These 90 samples were averaged for every scan (ideally there are 128 scans per data collection) and for each VIIRS detector. In addition, the 48 samples extracted from both the SD and OBC BB views were similarly averaged (note that calibration view data is reported in 14 bits while EV data is automatically truncated from 14 to 12 bits by VIIRS; in this analysis all calibration view data is first truncated to 12 bits to remove any potential bias). For each average, a three sigma outlier rejection was used. The OBC BB was maintained at ~ 292 K throughout the testing; as a result, the OBC BB data was used as a zero reference for both the EV and SD data.

The integrating sphere radiance and collimator irradiance were tracked in real-time by monitors (two monitors on the sphere and one monitor on the collimator). The output of each monitor was provided in volts, and was converted to either radiance or irradiance (the average of the two radiance monitors is used here) using NIST provided monitor calibration coefficients determined post-test. Output from each monitor was obtained about every 10 s. Linear interpolation was used to acquire the radiance or irradiance at the particular VIIRS time stamp associated with each scan.

Using Eqs. (2) and (3), the EV and SD responsivities were determined on a scan by scan basis. Since the EV and SD data was recorded at separate times, the scan averaged EV and SD responsivities were calculated for each data collection. These scan averaged responsivities were then substituted into Eq. (1), from which the responsivity ratio was determined for each three data collection cycle. The average of the two collection cycles per collimator position was then calculated.

The following sections will only discuss the results for HAM side A, but both HAM sides yield consistent results.

3.2 Data Quality

A number of data quality checks were performed during the processing of the data for the SD calibration. Listed below are the major findings of those checks.

Some of the collects did not contain the full expected 128 scans of VIIRS data (collects at positions 3 and 5, both at 852 nm). For those collects, the data was retained for those scans that appeared to be valid data (i.e. they were consistent with the data collects in which all scans were present).

The signal observed in the SD view when the EV was illuminated via the integrating sphere was negligible; in contrast, the response reported in the EV when the SD was illuminated via the collimator was between 2 - 3 dn for most cases. This is the possible result of scatter from the collimator reaching the EV, and as such had no real effect on the calibration. In addition, the data from the dark collects was analyzed and the resulting dn was negligible for all cases.

The standard deviation of the EV dn was determined over scans at each sample and also over samples at each scan (similarly for the SD dn). For the SD view, the two methods were comparable. However, for the EV, the standard deviation over samples was lower than the standard deviation over scans. This indicates that the integrating sphere had higher spatial stability than temporal stability (and that the measured SNR was closer to the true sensor SNR using the first method).

The stability of the sources was also tracked via their respective monitors. The two monitors on the integrating sphere showed some fluctuation over time (they both individually exhibited one sigma variation within about 0.3 % at 742 nm and 0.6 % at 852 nm); in addition, the two monitors varied in approximately the same manner. However, the monitors were offset from each other by about 0.4 % for 742 nm and 0.6 % for 852 nm. The collimator monitor recorded one sigma temporal variation of up to about 0.7 % (0.8 %) at 742 nm (852 nm) over a particular data collection.

The EV dn and monitor radiances had similar temporal trends, and as such the calculated EV responsivity at each scan was generally consistent over time. In contrast, the SD dn and collimator irradiance had different temporal dependencies, with the result being that the calculated SD responsivity was not necessarily constant over scans; examples of this behavior are plotted in Figures 1 – 4. The inability of the collimator monitor to effectively track the incident irradiance was a major source of uncertainty for the SD responsivity.

3.3 Responsivity Ratio Results

The derived M6 and M7 responsivity ratios for each detector and collimator position are shown in Figures 5 and 6, respectively. In the case of M6, all collimator positions were within ~2 % of one. In addition, the responsivity ratio tended to increase over detectors for all collimator positions (particularly positions 1 and 7). For M7, all positions were within ~4 % of unity, with the exception of position 7 which was between 4 and 6 % below one. Here the detector variation was again roughly increasing, but more uniformly over detector position than for M6. This detector trend likely resulted from detector dependence in the collimator uniformity correction (the RTA footprint on the SD was slightly different for each detector and band, which in turn required a slightly different collimator correction). The detector dependent collimator correction is left for future work. Although E2E testing was also conducted at 442 nm (M2) for collimator position 7, the digital response was too low to accurately determine the responsivity ratio (dn_{SD} ~ 6 and dn_{EV} ~ 15).

Measurement repeatability was investigated both on short time scales (minutes) and long time scales (hours). The collimator was positioned three times at roughly the same angle (positions 1, 4, and 5 in Table 1). The interval between positions 1 and 4 was about 6 hours and the interval between positions 4 and 5 was about 16 hours. For M6 (see the black, green, and yellow curves in Figure 5), the ratios were between 1.0 and 2.5 % above unity for all detectors for positions 4 and 5; however, the ratios derived from position 1 were lower (within 1.0 % of one). In addition, the detector variation was greater for position 1. In contrast, the M7 ratios derived from positions 1 and 5 were within 0.5 % of each other (although between 2 and 4 % below one), while the ratios from position 4 were within 1.5 % of one (see the black, green, and yellow curves in Figure 6).

In terms of short term stability, the E2E test was repeated for each collimator position twice within about 30 minutes (except position 5). The data from each individual collection cycle (SD, EV, dark) was used to derive a responsivity ratio. The comparison of the short term stability is shown in Figures 7 and 8 versus detector. Here the solid (dashed) lines indicate the first (second) measurement. For M6, positions 4 and 7 agreed to within 0.2 %, while positions 1, 2, 3, and 6 showed discrepancies up to 1 %. The ratios determined for M7 showed agreement to within 0.5 % for all positions except position 2, for which short term repeatability was about 2 %.

The discrepancies between the repeated measurements are largely understood by examining the underlying dn, radiance, and irradiance. In Table 3, the dn, radiance, and irradiance are listed for M6 detector 9 at each collimator position and measurement repeat (averaged over scans). For the EV, the dn increased when the radiance increased; however, this was not always the case for the SD measurements. Collimator positions 2, 3, and 6 actually had lower irradiance for the measurement with higher dn. This result also held when examining the SD on a scan basis. Thus the discrepancies in the repeatability measurements appear to be largely related to the accuracy of the irradiance monitor output.

The band averaged uncertainty estimates based on Eq. (7) are listed in Table 4 for all collimator positions. The BRF uncertainty was the largest contributor to the uncertainty for both M6 and M7 (at 1.09 %). The individual uncertainty contributors are listed in Table 5. Because the main source of error was not detector dependent, the variation of the uncertainty with detector was small for both bands. Note that the collimator uniformity correction uncertainty was not included (it is expected to be a major contributor).

Figures 9 and 10 show the band averaged responsivity ratio for each collimator position with the uncertainties shown in Table 4. The responsivity ratios were consistent with one for band M6 for most collimator positions (except position 4). For band M7, only collimator positions 2, 4, and 6 were consistent with one; all other positions were lower (especially position 7 which was much lower). The repeated collimator positions 1, 4, and 5 were consistent with each other (within uncertainties) for both bands. In addition, all short term repeated measurements agreed within the measured uncertainties.

4. Summary

- E2E testing represents an exploratory use of tunable lasers to characterize the VIIRS RSB on-orbit calibration cycle pre-launch.
- SD / EV responsivity ratios consistent with one for M6 (except for collimator position 4); Collimator positions 2, 4, and 6 are consistent with one for M7, but inconsistent for all other collimator positions.
- Measurement repeatability within 2 % for both bands, which is within uncertainties.
- Collimator irradiance monitor tracking of sensor response is inconsistent.

Acknowledgement

The sensor test data used in this document was provided by the BATC testing team. Approaches for data acquisition and data reductions, as well as data extraction tools were also provided by the Raytheon El Segundo team. We would like to thank the Raytheon El Segundo and BATC teams for their support. The data analysis tools were developed by the NICST team.

Table 1: E2E test data

Collimator Position	Date	Declination δ	Azimuthal φ	Wavelengths (Bands)	UAIDs	Collects
1	March 19, 2010	22.52	16.31	742 (M6), 852 (M7)	4742, 4744	1 – 6, 1 – 6
2	March 19, 2010	13.64	16.87	742 (M6), 852 (M7)	4746, 4747	1 – 6, 1 – 6
3	March 19, 2010	30.09	16.34	742 (M6), 852 (M7)	4749, 4750	1 – 6, 1 – 6
4	March 19, 2010	22.37	16.44	742 (M6), 852 (M7)	4751, 4752	1 – 6, 1 – 6
5	March 20, 2010	22.38	16.52	742 (M6), 852 (M7)	4753, 4754	1 – 3, 1 – 3
6	March 20, 2010	30.44	15.21	742 (M6), 852 (M7)	4755, 4756	1 – 6, 1 – 6
7	March 20, 2010	13.63	15.07	442 (M2), 742 (M6), 852 (M7)	4758, 4759, 4760	1 – 6, 1 – 6, 1 – 6

Table 2: Collimator uniformity corrections [4]

Collimator Position	1	2	3	4	5	6	7
M6	0.967	0.965	0.966	0.964	0.958	0.959	0.959
M7	0.940	0.937	0.933	0.936	0.924	0.926	0.933

Table 3: Short term repeatability for M6 detector 9 (HAM A).

Position	Measurement	E_{SD}	dn_{SD}	L_{EV}	dn_{EV}	η
1	1	5.084	648.2	0.1212	690.5	1.009
1	2	4.979	639.0	0.1216	693.7	1.004
2	1	4.845	615.4	0.1078	618.1	0.999
2	2	4.863	614.5	0.1083	620.3	1.003
3	1	5.096	655.7	0.1105	633.2	1.009
3	2	5.113	653.7	0.1097	628.0	1.015
4	1	4.862	615.4	0.1113	637.3	1.020
4	2	4.844	613.4	0.1116	639.4	1.020
6	1	6.316	777.9	0.1320	756.0	1.016
6	2	6.298	779.9	0.1322	757.4	1.011
7	1	6.502	800.4	0.1387	795.6	0.997
7	2	6.486	798.6	0.1379	791.8	0.998

Table 4: Band averaged responsivity ratio uncertainties

Collimator Position	1	2	3	4	5	6	7
M6	1.49	1.47	1.48	1.47	1.48	1.48	1.55
M7	1.73	1.72	1.68	1.73	1.70	1.82	1.74

Table 5: Individual uncertainty contributors for bands M6 and M7. p and a denote the precision and accuracy errors in L_{EV}.

Band	M6	M7
$u(dn_{EV})$	~0.4 %	~0.4 – 0.5 %
$u(dn_{SD})$	~0.4 – 0.6 %	~0.6 – 0.8 %
$u(L_{EV})(a)$	~0.3 %	~0.4 – 0.7%
$u(L_{EV})(p)$	~0.4 %	~0.6 %
$u(E_{SD})$	~0.1 – 0.7 %	~0.2 – 0.8 %
$u(BRF_{RTA})$	~1.1 %	~1.1 %
$u(\tau_{SAS})$	~0.2 %	~0.2 %
$u(\cos\theta_{SD})$	~0.4 %	~0.4 %
u(RVS)	~0.06 %	~0.06 %

Figure 1: M6 EV and SD scan dependent uncertainties (position 6)

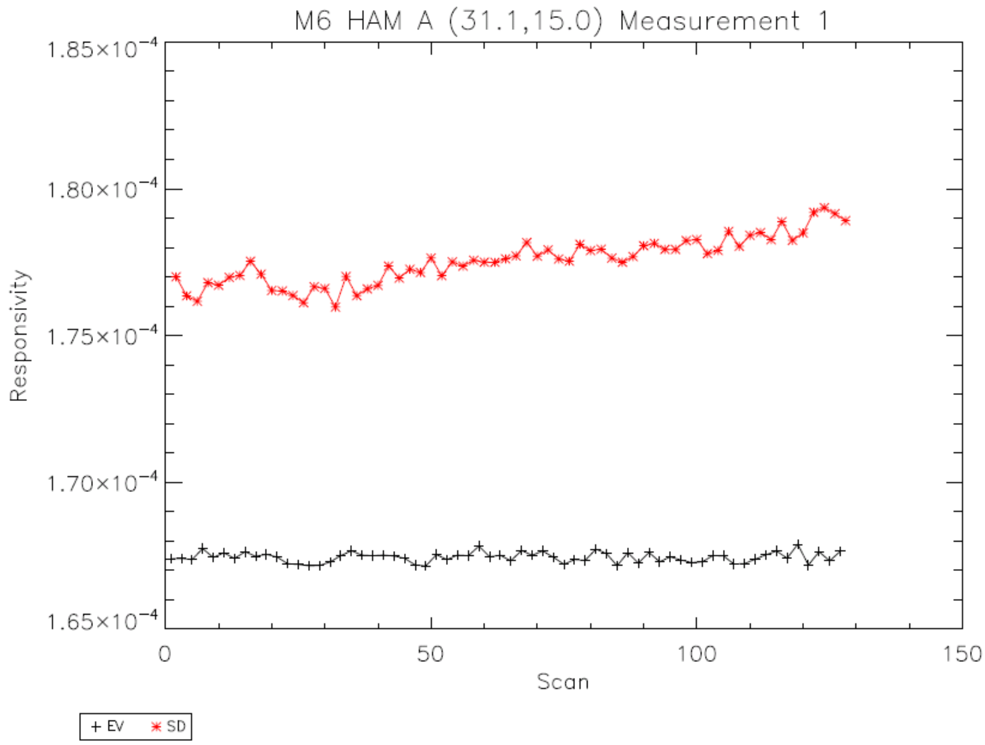

Figure 2: M6 EV and SD scan dependent uncertainties (position 7)

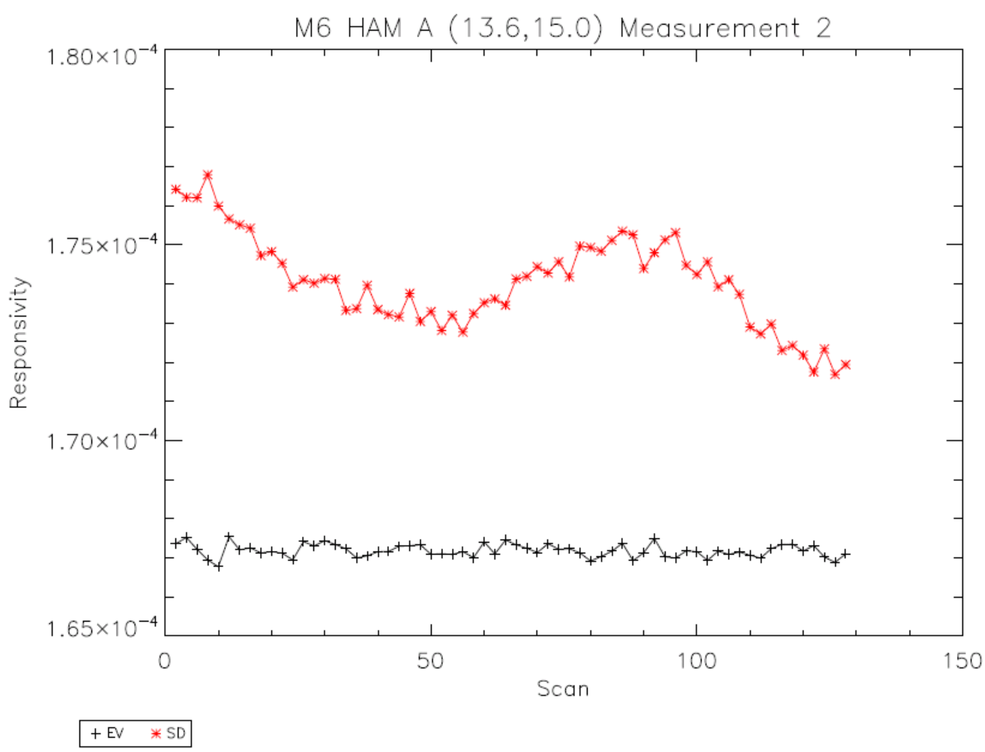

Figure 3: M7 EV and SD scan dependent uncertainties (position 6)

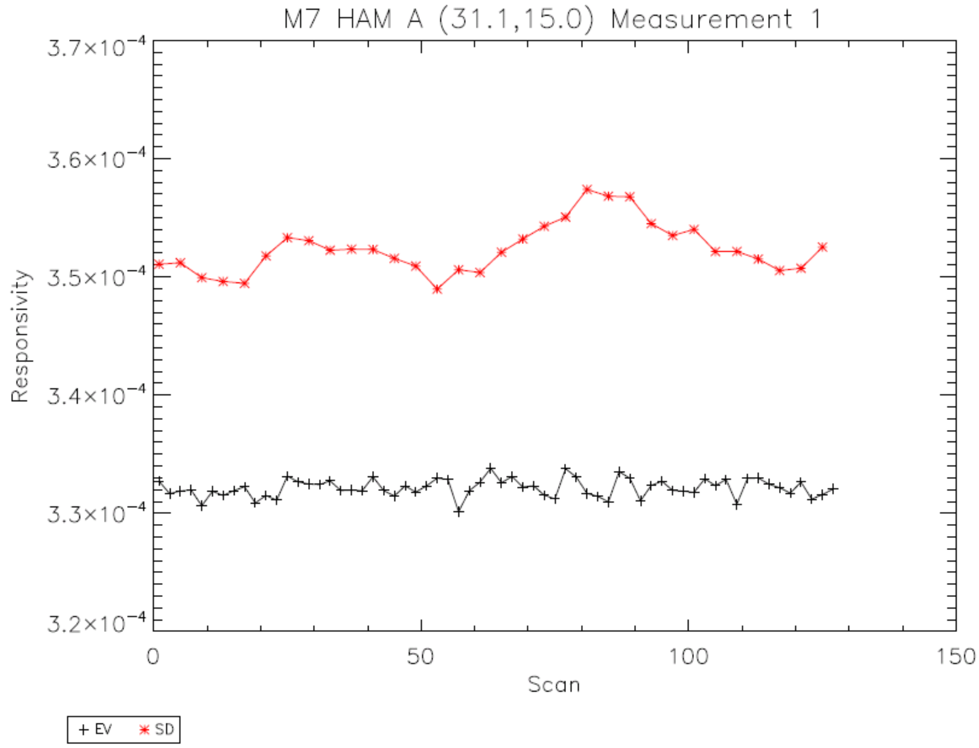

Figure 4: M7 EV and SD scan dependent uncertainties (position 7)

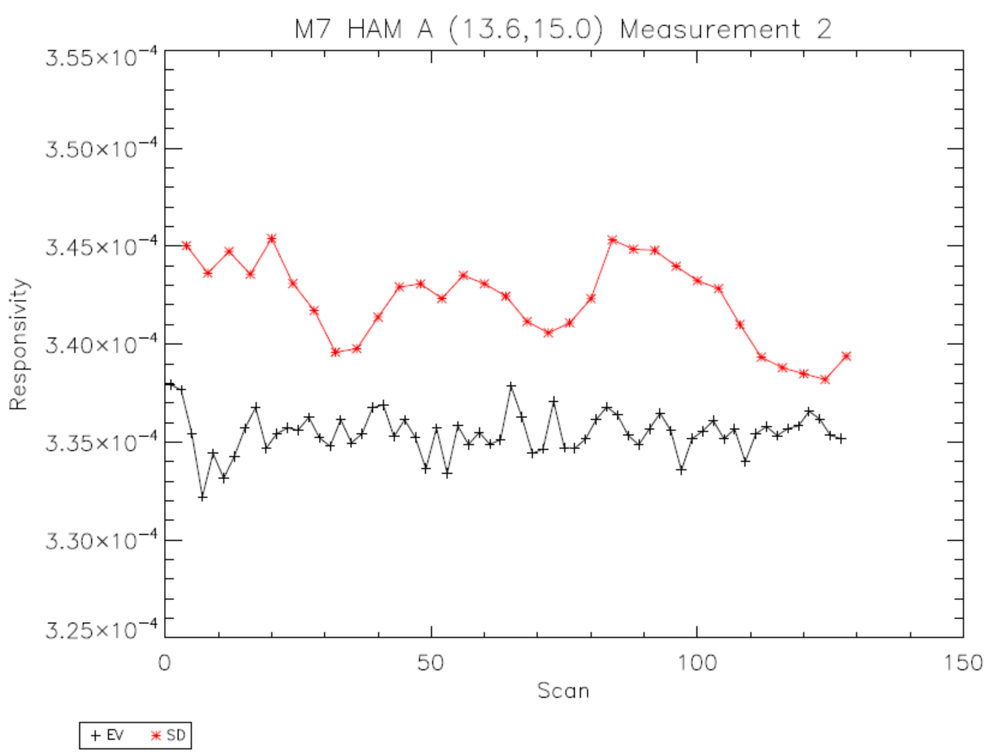

Figure 5: Responsivity ratios for M6

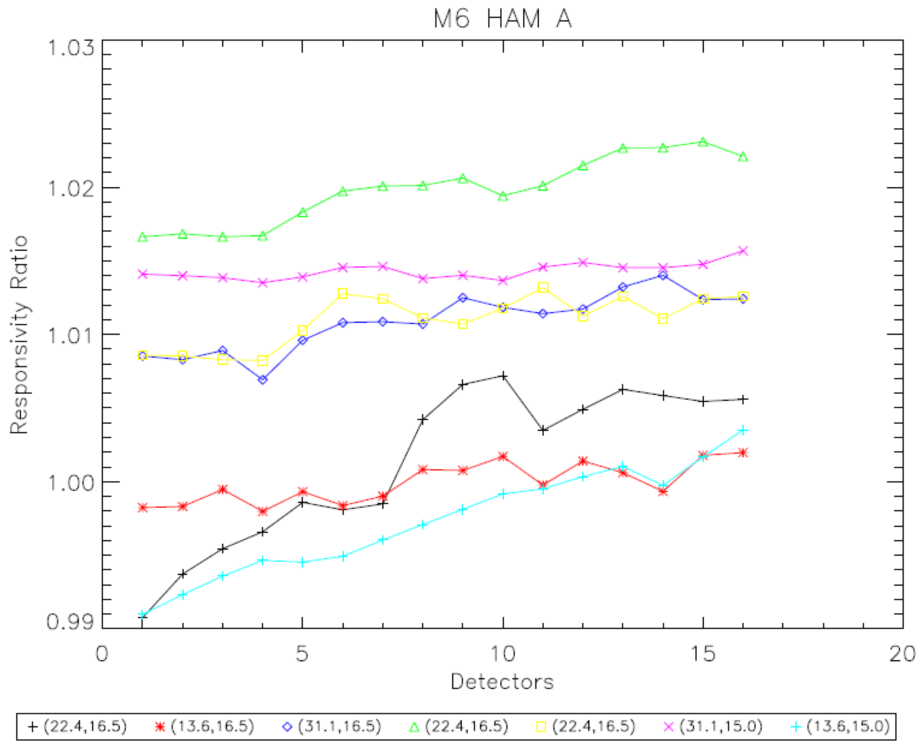

Figure 6: Responsivity ratios for M7

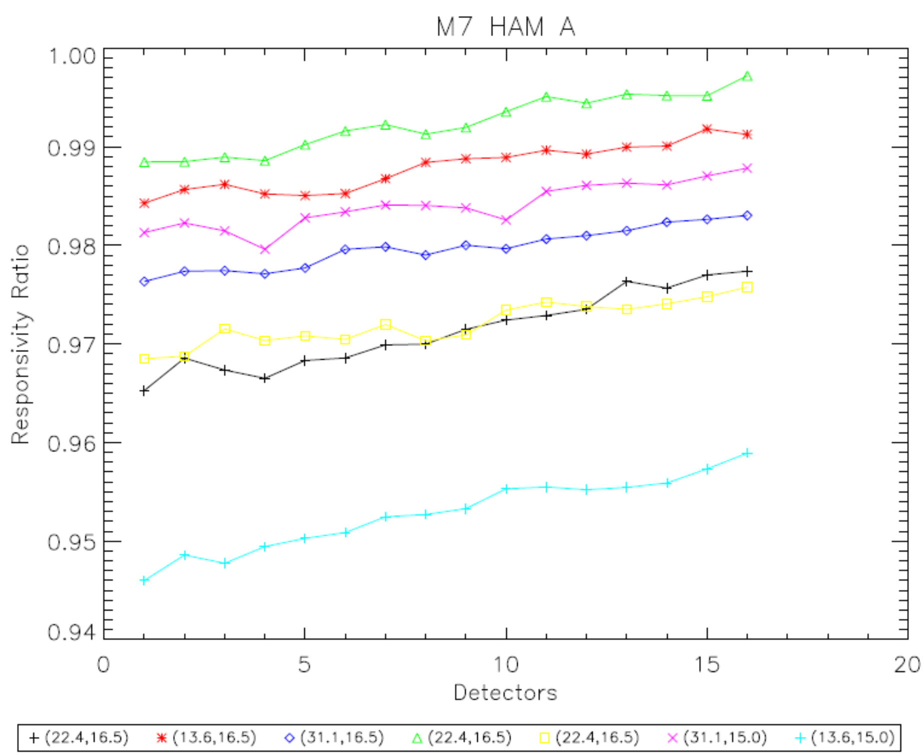

Figure 7: Short term repeatability for M6 responsivity ratios

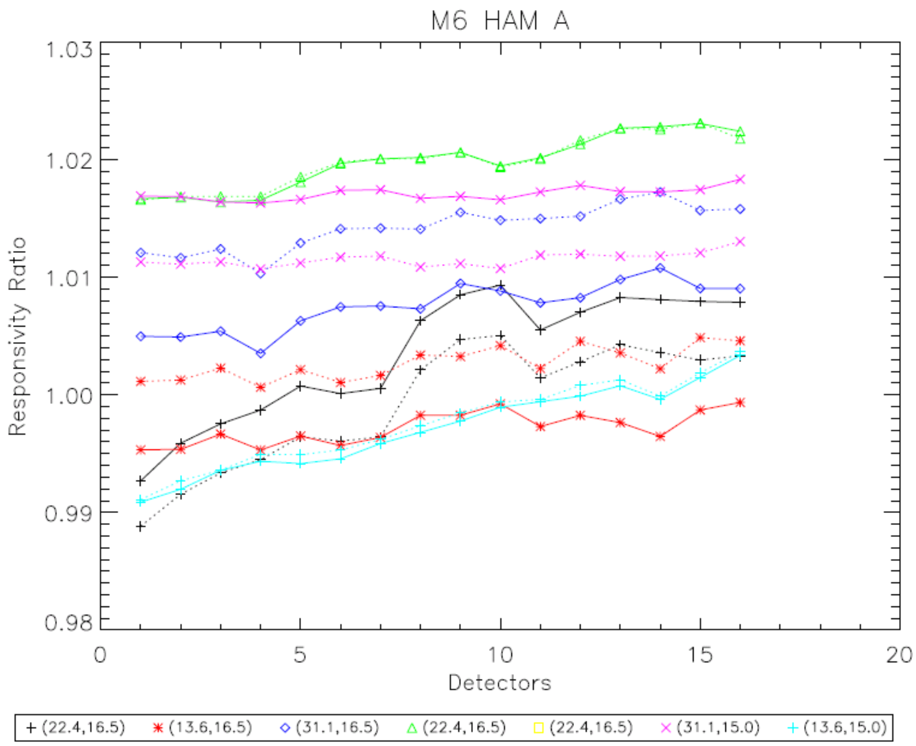

Figure 8: Short term repeatability for M7 responsivity ratios

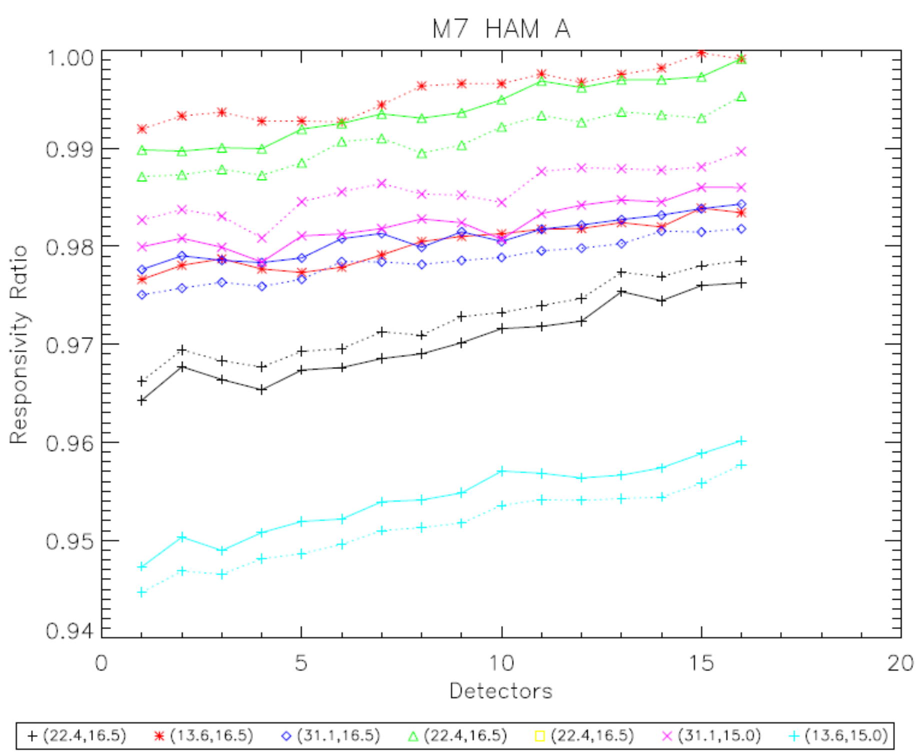

Figure 9: M6 band averaged responsivity ratios with uncertainties

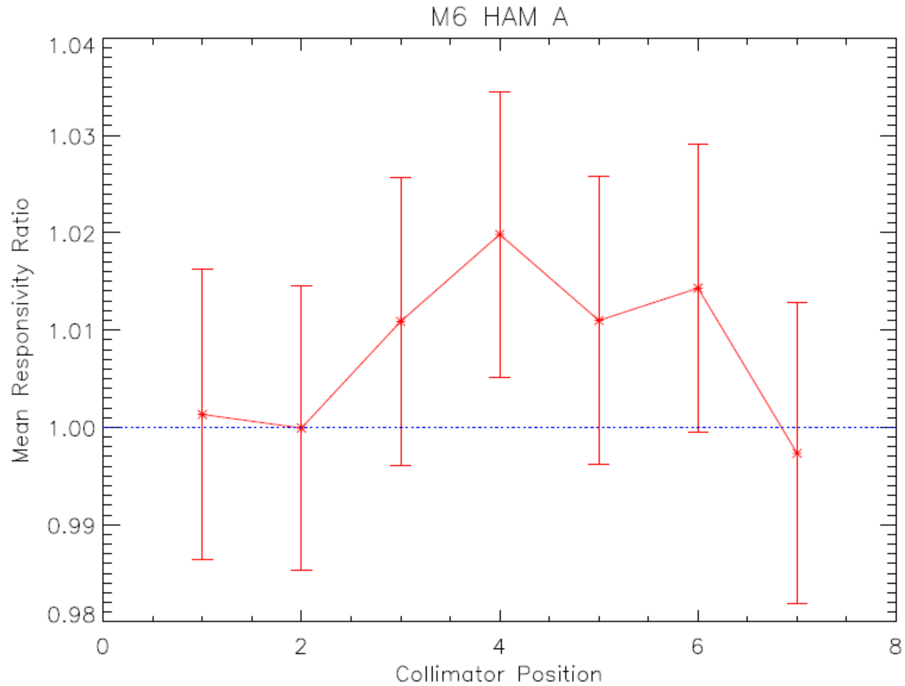

Figure 10: M7 band averaged responsivity ratios with uncertainties